Check for updates

The synthesis of polyaspartic acid derivative PASP-Im and investigation of its scale inhibition performance and mechanism in industrial circulating water

Xinyu Guo,[ac] Xiaowei Zhao,[ac] Yanhua Xu,[ac] Panpan Zhang,[ac] Yamin Cheng [ID] *[ac] and Ying Xu [ID] *[abc]

A polyaspartic acid derivative (PASP-Im) as a novel scale inhibitor was synthesized by a simple green synthesis route with polysuccinimide and iminodiacetic acid as the starting materials. The as-synthesized PASP-Im was characterized *via* nuclear magnetic resonance spectroscopy (^{1}H-NMR) and Fourier transform infrared spectrometry (FT-IR), and its scale inhibition performance was evaluated by a static scale inhibition method. Moreover, scanning electron microscopy, X-ray diffraction, X-ray photoelectron spectroscopy, and density functional theory computational studies were conducted to explore the scale inhibition mechanism of PASP-Im. The findings indicate that the as-synthesized PASP-Im exhibits better antiscale performance against the $CaCO_3$ deposits than the unmodified PASP because of the introduction of iminodiacetic acid group. It also can change the crystallization path of calcium carbonate from stable calcite to vaterite that is dispersible in water, thereby resulting in great changes in the morphology of the $CaCO_3$ scale. Furthermore, the O and N atoms in the negatively charged functional groups (such as $-NH_2$ and $-COOH$) of PASP-Im can interact with calcium ions to block the active growth point of $CaCO_3$ crystals, which also accounts for the excellent antiscale performance of PASP-Im. With new insights into the synergy between the functional groups of the antiscale molecule and scale-forming ions, this approach would be helpful towards the development of novel high-performance anti-scaling macromolecules.

1. Introduction

Industrialization is arousing significant concern about the shortage of freshwater resources,[1,2] which makes it imperative to explore the recycling of industrial water.[3,4] Unfortunately, the circulating cooling water containing a large amount of low-solubility salts tends to form inorganic scales on the pipe surfaces in the long-run, thereby causing damage to the water pipe and adding to the cost of production.[5–7] To overcome this drawback, some researchers tried to introduce small amounts of polymers as scale inhibitors into the industrial circulating water hoping to impair the scaling and significantly reducing the industrial water consumption.

Currently, available scale inhibitors include plant extracts, phosphorous compounds, polycarboxylic acids. Among them, the plant extracts, mainly consisting of polysaccharide and

protein-containing acidic groups can complex well with calcium ions to retard the formation of scales.[8–10] However, plant extracts as the scale inhibitor usually need an extremely high dosage to achieve the desired scale inhibition efficiency. Phosphorous compounds could be the most popular scale inhibitors because of their cost-effectiveness. Nevertheless, phosphorous compounds are often unfriendly to the environment and they could cause heavy eutrophication and increase in the biofouling of membrane systems.[11,12] Polycarboxylic acid additives, such as poly(acrylic acid), polymaleic acid and polyepoxysuccinic acid, usually have low calcium tolerance and can form insoluble calcium-polymer salts.[13–16] Therefore, it is urgent to develop green and highly-efficient scale inhibitors.

Non-toxic and biodegradable polyaspartic acid (PASP) without phosphorus could be a promising environmentally-friendly scale inhibitor if only its scale inhibition performance is significantly improved. In this respect, the introduction of functional groups possessing scale inhibition function onto the side chain of PASP through the amino-catalyzed ring-opening reaction could be encouraging.[14,17] An example of such side chain modification of PASP is available in our previous research,[18] but it is still challenging to design scale inhibitors

[a] College of Chemistry and Chemical Engineering, Henan University, Kaifeng 475004, China. E-mail: chengyamin16@126.com; hdccxu@126.com

[b] Engineering Research Center for Water Environment and Health of Henan, Zhengzhou University of Industrial Technology, Zhengzhou 451150, China

[c] Engineering Research Center for Industrial Recirculating Water Treatment, Henan University, Kaifeng 475004, China

with excellent anti-scale performance, low synthesis cost and weak environmental impact.

In this study, polyaspartic acid derivative (PASP-Im) is synthesized by a facile chemical modification method using polysuccinimide and iminodiacetic acid as the starting materials. The scale inhibition efficiency and mechanism of PASP-Im as a novel scale inhibitor are systematically investigated. This paper deals with the preparation of the PASP-Im scale inhibitor, and it also reveals the effects of the functional groups on the side chain of PASP on the formation of scale. This approach, hopefully, is to shed light on the design and synthesis of novel highly efficient green scale inhibitors in relation to their interaction mechanism with calcium carbonate crystals as well as their structure–activity correlation.

2. Materials and methods

2.1 Materials

Industrial grade polysuccinimide (PSI, $M_w = 7000$) was purchased from Wuhan Yuancheng Gongyi Technology Company Limited (Wuhan, China). Iminodiacetic acid was purchased from Saan Chemical Technology Company Limited (Shanghai, China). Anhydrous calcium chloride, disodium edetate and potassium hydroxide were purchased from Tianjin Komi Chemical Reagent Company Limited (Tianjin, China). Anhydrous sodium bicarbonate and sodium hydroxide were bought from Tianjin Deen Chemical Reagent Company Limited (Tianjin, China). Anhydrous ethanol was provided by Anhui Ante Food Company Limited (Anhui, China). Borax was bought from Tianjin Sailboat Chemical Reagent Technology Company Limited (Tianjin, China). Hydrochloric acid was purchased from China Pingmei Shenma Group Kaifeng Dongda Chemical Company Limited (Kaifeng, China). Deionized water (DI) was prepared at our laboratory and used as the solvent and for rinsing as well.

2.2 Preparation of PASP-Im

Certain amounts of PSI, iminodiacetic acid and DI water were mixed in a round-bottom flask and heated in a water bath at 60 °C for 1 h under stirring. The resultant mixture was allowed to react for 24 h after its pH was adjusted to 10 with a 10% sodium hydroxide solution. At the end of the reaction, the pH of the mixture was adjusted to 7–8 using hydrochloric acid, followed by precipitation with absolute ethanol for 12 h, purifying with a dialysis bag and drying at 60 °C to afford PASP-Im at a yield of about 76.0%.[19]

The structure of PASP-Im was characterized using a Fourier transform infrared spectrometer (VERTEX 70 FTIR spectrometer, Bruker Optics, Germany) and ^{1}H nuclear magnetic resonance (^{1}H-NMR; AVANCE 400 MHz NMR spectrometer, Bruker Optics, Germany). The molecular weight (M_w) of the as-prepared PASP-Im scale inhibitor was measured via gel permeation chromatography (PL-GPC50, Agilent, England). The acid value of PASP-Im and PASP was determined using a PHS-3E pH meter (Shanghai Electronic Scientific Instrument Company Limited; Shanghai, China).

2.3 Evaluation of the scale inhibition behavior of PASP-Im for CaCO₃

A static test was performed according to GB/T 16632-2008 (China) to examine the scale inhibition efficiency of the as-prepared PASP-Im for the $CaCO_3$ scale. In brief, the test solution (pH = 9) containing 240 mg L^{-1} of Ca^{2+} and 732 mg L^{-1} of HCO_3^- was prepared with DI water and heated at 80 °C for 10 h. Upon the completion of heating, the solution was filtered, and the filtrate was titrated with a ethylene diamine tetraacetic acid (EDTA) standard solution to determine the concentration of calcium ions.[18] The scale inhibition efficiency (η, %) of PASP-Im for the $CaCO_3$ scale is calculated using the eqn (1):

$$\eta = \frac{\rho_2 - \rho_1}{0.240 - \rho_1} \times 100\% \tag{1}$$

where ρ_1 and ρ_2 (mg mL^{-1}) are the concentrations of Ca^{2+} in the absence and presence of scale inhibitor, respectively; and the concentration of Ca^{2+} in the as-prepared calcium bicarbonate solution is 0.240 mg mL^{-1}.

2.4 Surface morphology observation of CaCO₃ crystals

The surface morphology of $CaCO_3$ crystals formed in the absence of antiscalant as well as in the presence of 100 mg L^{-1} PASP and 100 mg L^{-1} PASP-Im was observed using a scanning electron microscope (JSM-7610F, JOEL, Japan). X-ray diffraction (XRD) analysis (D8 Advance, Bruker Optics, Germany) was conducted to study the crystal structures of $CaCO_3$ in the scales. The chemical states of various elements in the $CaCO_3$ crystals obtained with and without PASP-Im were determined via X-ray photoelectron spectroscopy (XPS; ESCALAB 250Xi, Thermo, USA; monochromated Al K_α X-ray source, $h\nu = 1486.6$ eV) with contaminated carbon (C 1s = 284.8 eV) as the reference.

2.5 Quantum chemical study of the scale inhibition mechanism of PASP-Im

Non-local hybrid density functional B3LYP with the basis set 6-31 G of the Gaussian 09 program was adopted to conduct the complete optimization of the PASP-Im molecule.[20,21] The inhibition behavior of the PASP-Im additive was studied by a computational analysis based on the density functional theory (DFT).[22]

3. Results and discussion

3.1 Synthesis and structural characterization of PASP-Im

The PASP-Im antiscale agent was prepared using PSI (uncycloped polyaspartic acid) and iminodiacetic acid as raw materials. PSI is a highly reactive linear polyimide that can be easily activated by the amino group to form polyasparagine with side chains. The nucleophilic reaction of iminodiacetic acid and PSI under basic conditions affords the PASP-Im scale inhibitor (Fig. 1).

The FTIR spectra of PSI and PASP-Im are shown in Fig. 2. The absorbance bands of PSI at 1400 cm^{-1} and 1716 cm^{-1} are assigned to the symmetric stretching vibrations of C–N and C= O, respectively. The stretching vibration absorbance bands of
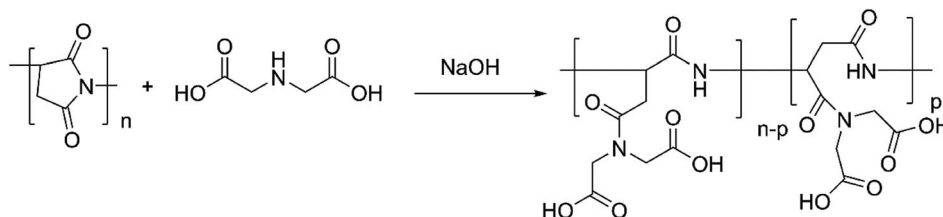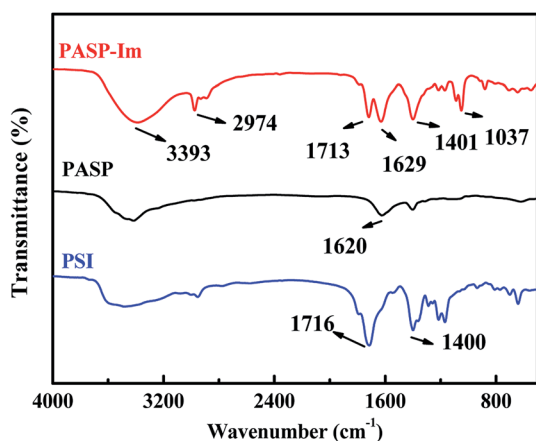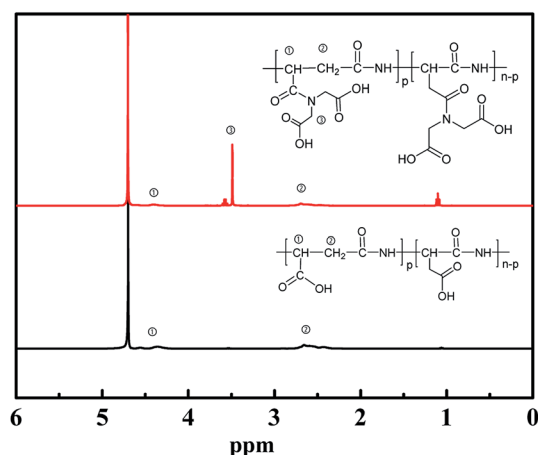
Fig. 1 Synthesis of the PASP-Im scale inhibitor.

Fig. 2 FTIR spectra of PASP-Im, PASP and PSI.

N–H and C=O as well as C–N in the amide bond of PASP-Im are located at 3393 cm^{-1}, 1629 cm^{-1} and 1401 cm^{-1}, respectively;[23] and the asymmetric stretching vibration peak of –CH$_2$– in the iminodiacetic acid is located at 2974 cm^{-1}.[24] Moreover, the absorbance peak at 1037 cm^{-1} is attributed to the stretching vibrations of the C–N species of amine and that at 1713 cm^{-1} is assigned to the C=O stretching vibrations of the carboxyl group.

Fig. 3 shows the ^{1}H-NMR spectra of PASP and PASP-Im in D$_2$O. The signals of PASP at 4.3 ppm and 2.6 ppm are attributed to –CH– and –CH$_2$–, respectively. Aside from the –CH– and –CH$_2$– signals of PASP, the new signal of PASP-Im at 3.5 ppm is ascribed to –CH$_2$– from iminodiacetic acid,[23] which proves the successful synthesis of PASP-Im.

3.2 Molecular weight distribution

As reported elsewhere, there is a close connection between the molecular weight distribution and scale inhibition performance.[13] The molecular weights of PASP-Im and PASP measured by GPC are listed in Table 1.

The as-prepared PASP-Im has a weight-average molecular weight (M_w) of 4445 and a number-average molecular weight (M_n) of 3908; and the PASP copolymer has an M_w/M_n ratio of 1.137. This means that the PASP-Im scale inhibitor has narrower molecular weight distribution as well as higher molecular weight and better dispersibility than PASP. The molecular weights of PASP-Im and PASP in combination with their FTIR and ^{1}H-NMR data confirm that the nucleophilic reaction of iminodiacetic acid and PSI under basic conditions indeed gives rise to the PASP-Im scale inhibitor successfully.

3.3 Acid value of PASP-Im

The acid values of PASP-Im and PASP with different concentrations are shown in Fig. 4. It can be seen that the pH values of PASP-Im and PASP solutions vary slightly with varying concentrations. The acid values of PASP-Im and PASP are about 7.0 and 8.5, respectively, which could be because the acidic groups of iminodiacetic acid can ionize to form hydrogen ions in the aqueous solution to reduce acid value.

3.4 Inhibition performance of PASP-Im against CaCO$_3$

Fig. 5 shows the scale-inhibition performance of PASP-Im for the calcium carbonate precipitate, as determined by the static scale inhibition test. The scale inhibition performance of PASP-Im tends to increase with increasing concentration, and it remains nearly constant when its concentration is beyond

Fig. 3 ^{1}H-NMR spectra of PASP-Im and PASP.

Table 1 Relative molecular mass and distribution of the PASP-Im and PASP copolymer

Samples	Parameters		
	M_n	M_w	PDI
PASP-Im	3908	4445	1.137
PASP	1778	2039	1.147

Fig. 4 Acid values of PASP-Im and PASP.

Fig. 6 Effect of pH on the scale inhibition performance of PASP-Im for $CaCO_3$.

Fig. 5 Variation in the inhibition efficiency of PASP-Im for $CaCO_3$ with concentration.

3.5 Characterization of calcium carbonate scales

The morphology change of the calcium carbonate crystals was identified *via* SEM in order to reveal the underlying mechanism of the macromolecular additives for impairing scaling. As shown in Fig. 7a, the $CaCO_3$ crystals formed in the absence of the scale inhibitor have regular shapes, smooth surfaces and compact crystal structures. After PASP is added, the resultant $CaCO_3$ crystals have an irregular morphology as well as increased granularity (Fig. 7b). The addition of PASP-Im leads to a great change in the shape as well as improves the dispersibility of the $CaCO_3$ crystals (Fig. 7c). This could be because the interaction between the carboxyl of PASP-Im and calcium ions blocks the active growth point of $CaCO_3$ crystals and causes great changes in the morphology of $CaCO_3$ scales,[25,26] which is also confirmed *via* relevant XRD analysis.

Fig. 8 shows the crystal structures of $CaCO_3$ scales analyzed *via* XRD. The diffraction peaks at $2\theta = 23.02°$, $29.43°$, $31.32°$, $36.02°$, $39.25°$, $39.36°$, $43.22°$, $47.50°$, $48.55°$ and $57.42°$ correspond to calcite, and those peaks at $2\theta = 26.10°$, $27.24°$, $33.20°$, $36.13°$, $41.17°$, $42.79°$, $45.80°$, $48.40°$ and $50.26°$ correspond to aragonite (Fig. 8a). This indicates that the primary crystals formed in the absence of scale inhibitors consist of calcite and aragonite.[27,28] After the addition of scale inhibitors, the diffraction peaks for vaterite emerge at $2\theta = 20.82°$, $24.81°$, $26.96°$, $32.65°$, $43.75°$ and $49.94°$ to accompany those of calcite. This demonstrates that calcite and vaterite are the main crystals formed in the presence of the scale inhibitor. Interestingly, the intensity of the diffraction peaks at $2\theta = 29.45°$ and $36.15°$, corresponding to the main growth crystal planes (104) and (110) of calcite, decreases after the addition of PASP-Im. This indicates that PASP-Im could effectively inhibit the growth of calcium carbonate crystals and block the conversion path of vaterite to calcite more effectively. Since calcite with a certain stable structure is the most stable thermodynamic crystal of calcium carbonate while aragonite crystal is liable to dispersion in water and scouring therein.[29–31] The addition of PASP-IM scale inhibitor promotes the formation of calcium carbonate from amorphous to aragonite and effectively prevents the deposition of scale.

30 mg L^{-1}. This means that the solubilization performance of PASP-Im for the calcium carbonate precipitate is enhanced with increasing concentration. The reason might be that the anions of PASP-Im can complex with more Ca^{2+} to retard the formation of theCaCO$_3$ precipitate, thereby resulting in a better scale inhibition performance at low concentrations. Particularly, at a concentration of 5 mg L^{-1}, the complexation and solubilization effect of PASP-Im for $CaCO_3$ are increased by 48% as compared with those of the PASP scale inhibitor. Since the best scale inhibition efficiency of PASP-Im was obtained at the concentration of 30 mg L^{-1}, the variations of its scale inhibition performance with a variety of factors were further investigated while its concentration was fixed at 30 mg L^{-1}.

Acidity is the key factor affecting the inhibition efficiency of the scale inhibitor. As shown in Fig. 6, the scale inhibition performance of PASP-Im in the pH range of 6–9 tends to decrease with the decrease in pH; and its scale inhibition efficiency is always above 70% in this pH range. This indicates that PASP-Im can more effectively reduce the scale formation rate of calcium carbonate than PASP under the same pH conditions. Alternatively, the PASP-Im scale inhibitor could be well applicable to the circulating water system.
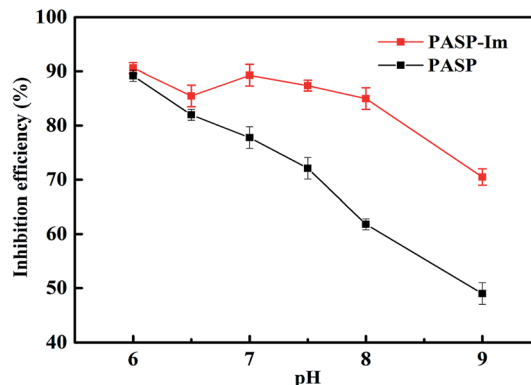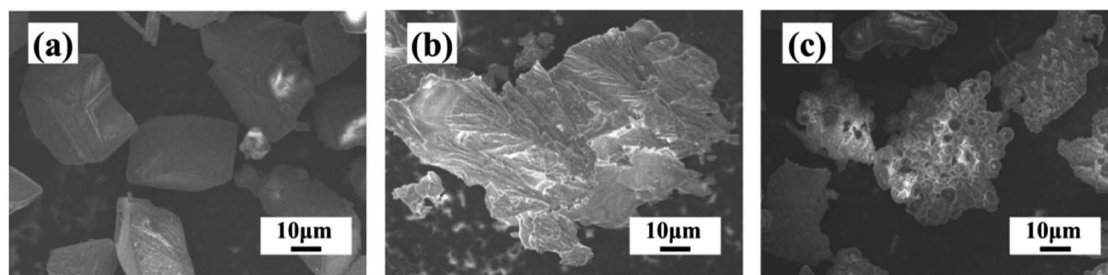
Fig. 7 SEM images of CaCO$_3$ crystals obtained without antiscalant (a) as well as with 30 mg L^{-1} of PASP (b) and 30 mg L^{-1} of PASP-Im (c).

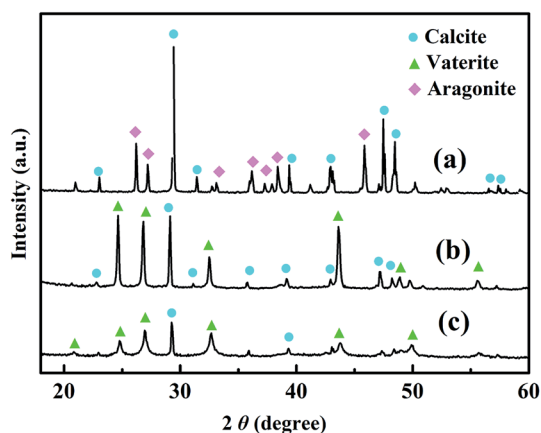Fig. 8 XRD patterns of CaCO$_3$ crystals without the copolymer (a), with 30 mg L^{-1} of PASP (b) and with 30 mg L^{-1} of the PASP-Im copolymer (c).

3.6 Scale inhibition mechanism of PASP-Im for calcium carbonate

XPS was conducted to explore the element composition of PASP-Im on the surface of calcium carbonate crystals. Fig. 9 shows the C 1s XPS spectra of CaCO$_3$ samples formed under different conditions. The two distinctive C 1s peaks at 289.57 eV and 286.06 eV correspond to C–O and C=O, respectively (Fig. 9a).[32] After the introduction of the PASP-Im scale inhibitor, new peaks assigned to the N–C=O group of amide emerge at 288.01 eV and 288.18 eV (Fig. 9b and c),[35,36] possibly due to the adsorption of the scale inhibitor on the calcite surface. Besides, after the addition of 30 mg L^{-1} PASP-Im, the C 1s peak assigned to N–C=O becomes much stronger than the same C 1s peak after

the addition of 10 mg L^{-1} PASP-Im, which implies that the increase in the scale inhibitor concentration might be favorable for its adsorption on the calcite surface. Moreover, the two peaks at 350.87 eV and 347.34 eV are attributed to Ca 2p$_{1/2}$ and Ca 2p$_{3/2}$ (Fig. 10a).[33,34] After the addition of 10 mg L^{-1} PASP-Im, the Ca 2p$_{1/2}$ and Ca 2p$_{3/2}$ peaks shift to 350.60 eV and 347.06 eV, respectively, and the introduction of 30 mg L^{-1} leads to a further shift of Ca 2p$_{1/2}$ and Ca 2p$_{3/2}$ peaks to 350.47 eV and 346.92 eV, respectively. This indicates that the introduction of the PASP-Im scale inhibitor causes changes in the chemical surroundings of Ca ion especially at a high dosage of the scale inhibitor. The reason might be that the functional groups of PASP-Im such as –NH$_2$ and –COOH can chelate with calcium ions, thereby increasing the electron density of the Ca ions. The XPS data, in combination with the aforementioned SEM and XRD results, demonstrate that PASP-Im can influence the conversion pathway of calcium carbonate and inhibit its crystal growth.

The optimized structure of PASP-Im based on quantum chemistry calculations is shown in Fig. 11. All the O and N atoms of PASP-Im have a high degree of a negative charge, which means that PASP-Im can provide Ca^{2+} with a large amount of binding sites.[35–39] As a result, the N and O atoms in the molecular structure of PASP-Im can be well bound to Ca^{2+} ion, thereby inhibiting the growth of calcium carbonate crystals as well as the formation of calcium carbonate scales.

During the long-term service of water pipelines, calcium carbonate crystals can form stable calcite deposits on the pipe surface. When PASP-Im is dissolved in water, the negatively charged functional groups of the PASP-Im chain, such as –NH$_2$ and –COOH, can combine with positively-charged metal ions to
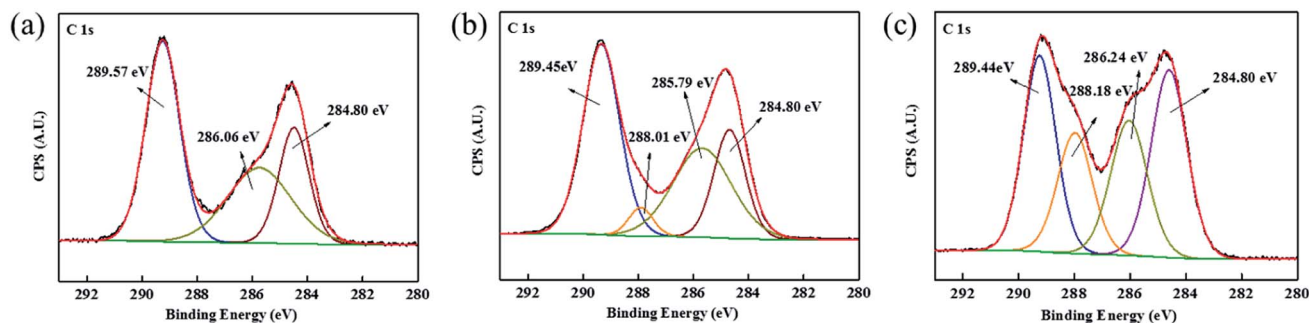

Fig. 9 C 1s XPS spectra of CaCO$_3$ samples formed in the blank (a) as well as in the presence of 10 mg L^{-1} PASP-Im (b) and 30 mg L^{-1} PASP-Im (c).

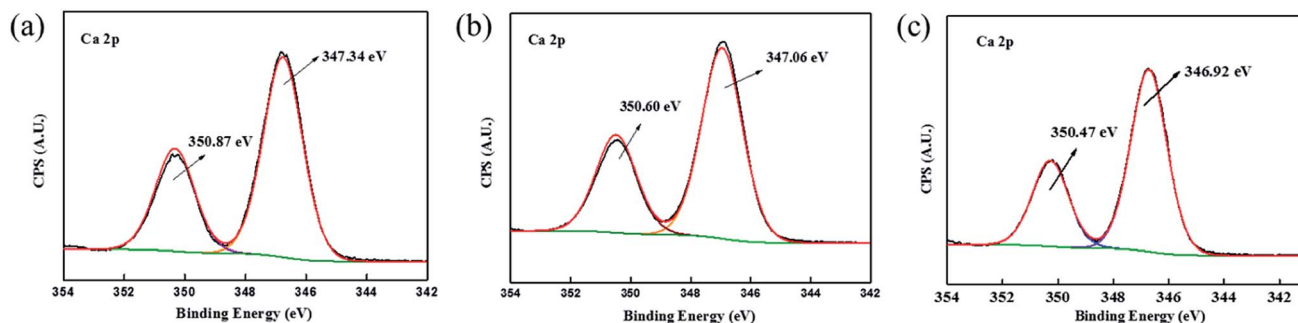**Fig. 10** Ca 2p XPS spectra of CaCO$_3$ samples formed in the blank (a) as well as in the presence of 10 mg L^{-1} PASP-Im (b) and 30 mg L^{-1} PASP-Im (c).
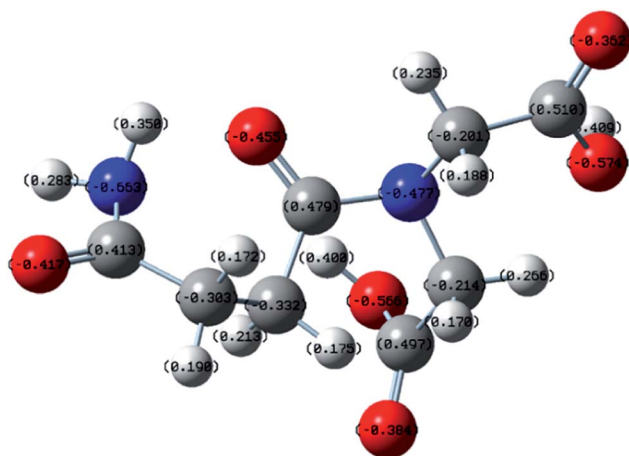

Fig. 11 Arrangements of charges in the PASP-Im monomer molecule.

form unstable calcium carbonate crystals and reduce the formation of calcite. Meanwhile, PASP-Im adsorbed on the calcium carbonate scale can increase the repulsive force between particles, thereby preventing the inter-particle binding and impairing the deposition of the mineral scales. In summary, the functional groups in the molecular structure of

the scale inhibitor play a key role in regulating its scale inhibition efficiency, and the grafting of N- and O-containing heteroatom functional groups with PASP could shed light on the development of novel highly efficient scale inhibitor (Fig. 12).

4. Conclusions

PASP-Im, a polyaspartic acid derivative, as a scale inhibitor for industrial circulating water is synthesized by a simple and green synthesis method. Characterizations *via* SEM and XPS as well as DFT calculations demonstrate that the as-synthesized PASP-Im exhibits better antiscale performance against the deposit of CaCO$_3$ scales than the unmodified PASP. It also can change the crystallization path of calcium carbonate from stable calcite to vaterite, which is dispersible in water, leading to great changes in the morphology of CaCO$_3$ scales. This is because, on the one hand, the PASP-Im can significantly change the shape of the calcium carbonate scales and block their crystallization path in the early stage, thereby retarding the formation of calcite. On the other hand, the O and N atoms in the negatively charged functional groups of PASP-Im, including –NH$_2$ and –COOH, can interact with Ca^{2+} ions to block the active growth points of CaCO$_3$ crystals and retard the formation of CaCO$_3$ scales. The present approach, with new insights into the synergy between
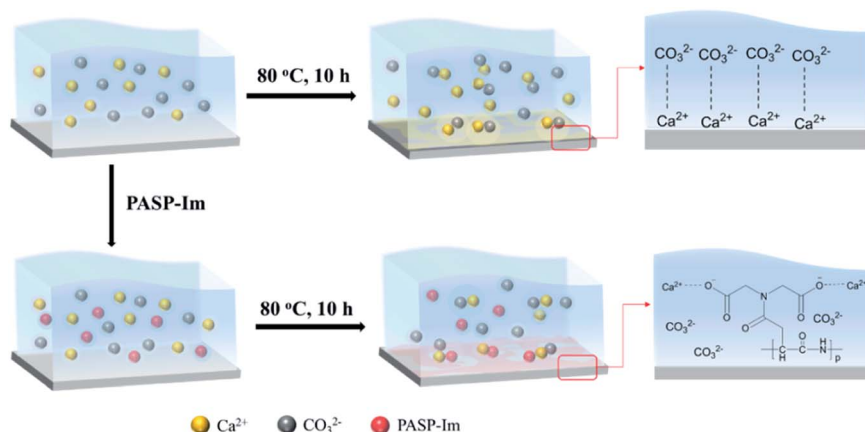

Fig. 12 Schematic of the scale inhibition mechanism of PASP-Im.

the functional groups of the antiscale molecule and scale-forming ions could provide a reference for the development of highly efficient anti-scaling macromolecules.

Conflicts of interest

There are no conflicts to declare.

Acknowledgements

References

1 I. Haddeland, J. Heinke, H. Biemans, S. Eisner, M. Florke, N. Hanasaki, M. Konzmann, F. Ludwig, Y. Masaki, J. Schewe, T. Stacke, Z. D. Tessler, Y. Wada and D. Wisser, *Proc. Natl. Acad. Sci. U. S. A.*, 2014, **111**, 3251–3256.

2 B. Randolph and P. Troy, *Environ. Sci. Policy*, 2008, **11**, 441–455.

3 Z. Zuo, W. Yang, K. Zhang, Y. Chen, M. Li, Y. Zuo, X. Yin and Y. Liu, *J. Colloid Interface Sci.*, 2020, **562**, 558–566.

4 A. Al Helal, A. Soames, R. Gubner, S. Iglauer and A. Barifcani, *J. Colloid Interface Sci.*, 2018, **509**, 472–484.

5 J. Li, Y. Zhou, Q. Yao, T. Wang, A. Zhang, Y. Chen, W. Wu and W. Sun, *Ind. Eng. Chem. Res.*, 2017, **56**, 2624–2633.

6 B. Zhang, C. He, C. Wang, P. Sun, F. Li and Y. Lin, *Corros. Sci.*, 2015, **94**, 6–20.

7 S. L. P. Wolf, K. Jähme and D. Gebauer, *CrystEngComm*, 2015, **17**, 6857–6862.

8 E. Ituen, O. Akaranta, A. James and S. Sun, *Environ. Sci. Policy*, 2017, **11**, 12–18.

9 T. Lourteau, H. Berriche, K. Kécili, V. Heim, D. Bricault, M. Litaudon, X. Cachet, F. Roussi, H. Perrot, O. Horner and H. Cheap-Charpentier, *J. Cryst. Growth*, 2019, **524**, 125161.

10 M. K. Nayunigari, A. Maity, S. Agarwal and V. K. Gupta, *J. Mol. Liq.*, 2016, **214**, 400–410.

11 T. Jain, E. Sanchez, E. Owens-Bennett, R. Trussell, S. Walker and H. Liu, *Environ. Sci.: Water Res. Technol.*, 2019, **5**, 1285–1294.

12 A. Sheikhi, A. Kakkar and T. G. M. van de Ven, *J. Mater. Chem. A*, 2018, **6**, 10189–10195.

13 S. A. Ali, I. W. Kazi and F. Rahman, *Desalination*, 2015, **357**, 36–44.

14 Y. Gao, L. Fan, L. Ward and Z. Liu, *Desalination*, 2015, **365**, 220–226.

15 J. Hao, L. Li, W. Zhao, X. Wu, Y. Xiao, H. Zhang, N. Tang and X. Wang, *ACS Appl. Mater. Interfaces*, 2019, **11**, 9277–9282.

16 H. Huang, Q. Yao, H. Chen and B. Liu, *RSC Adv.*, 2016, **6**, 92943–92952.

17 X. Sun, W. Song and L. Liu, *J. Mol. Catal. B: Enzym.*, 2015, **121**, 1–8.

18 B. Zhang, D. Zhou, X. Lv, Y. Xu and Y. Cui, *Desalination*, 2013, **327**, 32–38.

19 S. Shi, Y. Wu, Y. Wang, J. Yu and Y. Xu, *RSC Adv.*, 2017, 7, 36714–36721.

20 J. Kawano, S. Maeda and T. Nagai, *Phys. Chem. Chem. Phys.*, 2016, **18**, 2690–2698.

21 D. Yin, L. Yang, X. Niu, Y. Ma, M. Liu, X. Sun, B. Gao and B. Tan, *Colloids Surf., A*, 2020, **591**, 124516.

22 Y. Ji, B. Xu, W. Gong, X. Zhang, X. Jin, W. Ning, Y. Meng, W. Yang and Y. Chen, *J. Taiwan Inst. Chem. Eng.*, 2016, **66**, 301–312.

23 C. Chai, Y. Xu, D. Li, X. Zhao, Y. Xu, L. Zhang and Y. Wu, *Prog. Org. Coat.*, 2019, **129**, 159–170.

24 X. Guo, F. Qiu, K. Dong, X. Zhou, J. Qi, Y. Zhou and D. Yang, *J. Ind. Eng. Chem.*, 2012, **18**, 2177–2183.

25 M. F. Sousa and C. A. Bertran, *J. Colloid Interface Sci.*, 2014, **420**, 57–64.

26 K. Popov, M. Oshchepkov, E. Afanas'eva, E. Koltinova, Y. Dikareva and H. Rönkkömäki, *Colloids Surf., A*, 2019, **560**, 122–129.

27 X. Yuan, S. Dong, Q. Zheng, W. Yang and T. Huang, *Chem. Eng. J.*, 2020, **389**, 124296.

28 C. Cui and S. Zhang, *New J. Chem.*, 2019, **43**, 9472–9482.

29 K. D. Demadis and S. D. Katarachia, *Phosphorus, Sulfur, Silicon Relat. Elem.*, 2004, **179**, 627–648.

30 J. Chen, L. Xu, J. Han, M. Su and Q. Wu, *Desalination*, 2015, **358**, 42–48.

31 H. Wang, Y. Zhou, Q. Yao, S. Ma, W. Wu and W. Sun, *Desalination*, 2014, **340**, 1–10.

32 T. L. Barr and S. Seal, *J. Vac. Sci. Technol., A*, 1995, **13**, 1239–1246.

33 W. J. Landis and J. R. Martin, *J. Vac. Sci. Technol., A*, 1984, **2**, 1108–1111.

34 S. L. Stipp and M. F. Hochella Jr., *Geochim. Cosmochim. Acta*, 1991, **55**, 1723–1736.

35 A. Szcześ, M. Czemierska and A. Jarosz-Wilkołazka, *J. Solid State Chem.*, 2016, **242**, 212–221.

36 S. Li, Q. Qu, L. Li, K. Xia, Y. Li and T. Zhu, *Water Res.*, 2019, **166**, 115094.

37 Q. Yang, Y. Liu, A. Gu, J. Ding and Z. Shen, *J. Colloid Interface Sci.*, 2001, **240**, 608–621.

38 E. Weber, D. Levy, M. Ben Sasson, A. N. Fitch and B. Pokroy, *RSC Adv.*, 2015, **5**, 98626–98633.

39 M. Pons-Jiménez, R. Hernández-Altamirano, R. Cisneros-Dévora, E. Buenrostro-González, R. Oviedo-Roa, J.-M. Martínez-Magadán and L. S. Zamudio-Rivera, *Fuel*, 2015, **149**, 66–77.